ELSEVIER

Nuclear Physics A 617 (1997) 131–147

NUCLEAR PHYSICS A

Tilted rotation of triaxial nuclei

S. Frauendorf, Jie Meng [1]

Institut für Kern- und Hadronenphysik, Forschungszentrum Rossendorf e.V., PF 510119, 01314 Dresden, Germany

Received 14 November 1996

Abstract

The Tilted Axis Cranking theory is applied to the model of two particles coupled to a triaxial rotor. Comparing with the exact quantal solutions, the interpretation and quality of the mean field approximation is studied. Conditions are discussed when the axis of rotation lies inside or outside the principal planes of the triaxial density distribution. The planar solutions represent $\Delta I = 1$ bands, whereas the aplanar solutions represent pairs of identical $\Delta I = 1$ bands with the same parity. The two bands differ by the chirality of the principal axes with respect to the angular momentum vector. The transition from planar to chiral solutions is evident in both the quantal and the mean field calculations. Its physical origin is discussed. © 1997 Elsevier Science B.V.

PACS: ...
Keywords: Tilted axis cranking; Triaxiality; Chirality

1. Introduction

The orientation of the deformed density distribution relative to the (space-fixed) angular momentum vector becomes a useful concept at high spin. Tilted Axis Cranking (TAC) [1] is the version of the mean field theory that permits the calculation of the orientation of the deformed field in space together with the parameters that define its shape. Since its introduction [2], TAC has turned out to be a reliable approximation to calculate both energies and intra band transition probabilities (cf. Refs. [3–6]). These applications are restricted to axial or slightly triaxial nuclei. In such cases the angular momentum lies in one of the principal planes (PP) defined by the principal axes

[1] Also at Institute of Theoretical Physics, Chinese Academy of Science, Beijing 100080, PR China. Present address: Alexander von Humboldt fellow, Physik-Department der Technischen Universität München, D-85747 Garching, Germany.

PII S0375-9474(97)00004-3

(PA) of the deformed density distribution. The interpretation of such *planar* solutions is discussed in Refs. [1,2]. In triaxial nuclei there exists the possibility of *aplanar* solutions, where the angular momentum vector does not lie in one of the PP. The existence of such solutions for a fixed triaxial shape has first been demonstrated in Ref. [8], however its interpretation remained open. In this paper such interpretation is given and the consequences of substantial triaxiality for tilted rotation are investigated. A system of two particles coupled to a triaxial rotor (Particle Rotor Model, PRM) is studied and exact quantal solutions are found numerically. They are compared with the approximate solutions of the TAC approximation to this model system. Such approach has turned out to be quite instructive in the axial case, permitting a check of the accuracy of the TAC approximation and a refinement of the interpretation of this approach [9]. A preliminary report on the present study has been given in Ref. [7].

2. TAC and PRM basics

In TAC one seeks HF or HFB solutions that rotate uniformly about the angular momentum axis $\boldsymbol{J}$ that is tilted with respect to the PA 1, 2 and 3 of the deformed density distribution. The orientation of the rotational axis with respect to the PA is described by the two polar angles ϑ and φ, which are illustrated in the upper panel of Fig. 1. The system of PA may be defined by means of the quadrupole moments of the density distribution Q_μ. In the PA frame, the intrinsic quadrupole moments Q'_1 and Q'_{-1} must be equal to zero and $Q'_2 = Q'_{-2}$. The orientation of the density distribution in the lab frame x, y, and z is described by the three Euler angles ψ, ϑ and φ, which are illustrated in the lower panel of Fig. 1. The quadrupole moments in the intrinsic PA and the lab frame are connected by the relation

$$Q_\mu = D^{*2}_{0\lambda}(\psi,\vartheta,\varphi)Q'_0 + (D^{*2}_{2\mu}(\psi,\vartheta,\varphi) + D^{*2}_{-2\mu}(\psi,\vartheta,\varphi))Q'_2. \tag{1}$$

If the z-axis is chosen as the axis of rotation, the angles ϑ and φ describing the orientation in the two frames are the same.

In order to find these orientation angles one diagonalizes the single-particle Routhian

$$h' = h_{\mathrm{def}} - \boldsymbol{\omega}\cdot\boldsymbol{j}, \tag{2}$$

$$\boldsymbol{\omega} = (\omega\sin\vartheta\sin\varphi, \omega\sin\vartheta\cos\varphi, \omega\cos\vartheta), \tag{3}$$

where h_{def} is the Hamiltonian of the deformed field. It is obtained in a self-consistent way from a rotational-invariant two-body Hamiltonian H and the particle density generated by (2).

Each configuration $|\ \rangle$ constructed from the single-particle or quasiparticle eigenstates of the Routhian (2) corresponds to a rotational band. Each band has its individual tilt that is determined by minimizing the total Routhian

$$E'(\omega,\vartheta,\varphi) = \langle H - \boldsymbol{\omega}\cdot\boldsymbol{j}\rangle \tag{4}$$

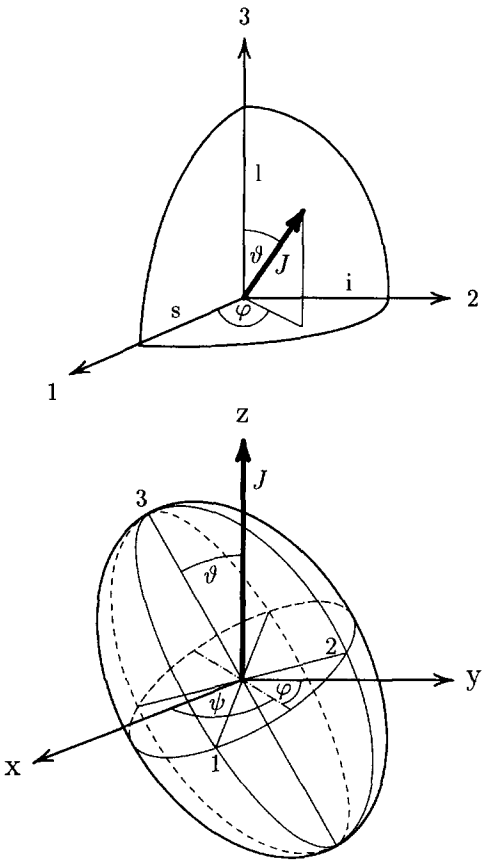

Fig. 1. Orientation of the axis of rotation (J, displayed as the heavy vector) with respect to the principal axes of the triaxial density distribution (upper panel) and orientation of the triaxial density distribution in the lab frame (lower panel). The long, intermediate and short semi-axes of the density distribution are labeled by l, i and s, respectively.

with respect to ϑ and φ at fixed ω. At the minimum the angular momentum vector

$$J = \langle j \rangle, \tag{5}$$

and the angular velocity $\boldsymbol{\omega}$ are parallel, $(J|\boldsymbol{\omega})$ [1]. These self-consistency equations must be complemented by additional ones that determine the shape of the density distribution. It is noted that due to the rotational invariance of the two-body Hamiltonian H there is a whole set of degenerate self-consistent solutions that differ from each other by the angle ψ in the lab frame. In Ref. [1], the TAC theory is described in more detail for the QQ-model Hamiltonian, for which it is particularly transparent.

In this paper we do not employ the microscopic TAC approach. Being mainly interested in the interpretation of the mean field solutions, we study the simple model system of a $h_{11/2}$ proton particle or hole and a $h_{11/2}$ neutron hole coupled to a triaxial rotor. The shape is assumed to be given. The Hamiltonian of this PRM is

$$H = h_{\rm def} + \sum_{\nu=1}^{3} \frac{(I_\nu - j_\nu)^2}{2\mathcal{J}_\nu}. \tag{6}$$

For the moments of inertia the ratios of irrotational flow are assumed, [2]

$$\mathcal{J}_\nu = \mathcal{J} \sin\left(\gamma - \frac{2\pi}{3}\nu\right)^2. \tag{7}$$

For $\gamma = -30°$, the moment of inertia $\mathcal{J}_2$ is larger than $\mathcal{J}_1 = \mathcal{J}_3$. The Hamiltonian of the deformed field is $h_{\rm def} = \pm h_p - h_n$, where the plus sign refers to particles and the minus to holes. We use the single-particle Hamiltonian of a high j particle, as given by

$$h = \frac{1}{2}C\left\{\left(j_3^2 - \frac{j(j+1)}{3}\right)\cos\gamma + \frac{1}{2\sqrt{3}}[j_+^2 + j_-^2]\sin\gamma\right\}. \tag{8}$$

In the calculation we take $C = 0.25$ MeV and $\mathcal{J} = 40$ MeV^{-1}, corresponding to a deformation of $\beta \approx 0.25$. More details concerning the PRM can be found in Ref. [9].

The TAC approximation to the PRM consists in two assumptions:

(i) The operator $\boldsymbol{I}$ of the total angular momentum is replaced by the classical vector $\boldsymbol{J}$;

(ii) $\langle \boldsymbol{j}^2 \rangle = \langle \boldsymbol{j} \rangle^2$.

Assumption (i) expresses the semi-classical treatment of the total angular momentum in the TAC approximation and assumption (ii) the mean field character of this approach.

The wave function $|\rangle$ is the product of the proton and neutron wave functions. Taking the expectation value of the Hamiltonian (6) with $|\ \rangle$ and using the approximations (i) and (ii), one obtains the energy

$$E = \langle h_{\rm def} \rangle + \sum_{\nu=1}^{3} \frac{(J_\nu - \langle j_\nu \rangle)^2}{2\mathcal{J}_\nu}. \tag{9}$$

Minimizing it with respect to $|\ \rangle$ results in the TAC Routhian (2) determining $|\ \rangle$, where the angular velocity $\boldsymbol{\omega}$ is given by

$$\omega_\nu = \frac{R_\nu}{\mathcal{J}_\nu}, \qquad R_\nu = J_\nu - \langle j_\nu \rangle. \tag{10}$$

Here, we have introduced the classical vector $\boldsymbol{R}$ of the rotor angular momentum.

The solution of this eigenvalue problem provides the wave function and energy as functions of $\boldsymbol{J}$. The orientation of the rotational axis is not yet fixed. It is found by minimizing the energy (9) with respect to the three components J_ν subject to the subsidiary condition that $J = \sqrt{J_1^2 + J_2^2 + J_3^2}$ is constant. Taking into account the stationarity of $|\ \rangle$, one obtains the two equations

$$\frac{\omega_1}{\omega_2} = \frac{J_1}{J_2}, \qquad \frac{\omega_1}{\omega_3} = \frac{J_1}{J_3}, \tag{11}$$

[2] We use the "Lund convention" to introduce the triaxiality parameter γ.

i.e. the TAC condition that $\boldsymbol{\omega}$ and $\boldsymbol{J}$ must be parallel. This is equivalent to finding the orientation of the rotational axis by minimizing the total Routhian

$$E' = \langle h' \rangle - \frac{1}{2} \sum_{\nu=1}^{3} \mathcal{J}_\nu \omega_\nu^2, \tag{12}$$

with respect to the angles ϑ and φ, where the components ω_ν are given by Eq. (3).

3. Discussion

In the case of substantial triaxiality of the nuclear density distribution, there exist two possibilities:

(i) The rotational axis $(\boldsymbol{J}|\boldsymbol{\omega})$ lies in one of the three PP 1–2, 1–3 or 2–3. We call such a solution *planar*.

(ii) The rotational axis does not lie in one of the PP. We call such a solution *aplanar*.

For our model system the appearance of the two types of solutions can be easily understood. The high j particles tend to align with the 1-axis because their torus like density distribution has the maximal overlap with the triaxial core in the 2–3 plane. The high j holes tend to align with the 3-axis because their dumbbell-like density distribution has maximal overlap if its symmetry axis is parallel to the long axis. For $\gamma = -30°$, the moment of inertia $\mathcal{J}_2$ is the largest and it is favorable to built up the core angular momentum along the 2-axis. Thus, if a proton hole and a neutron hole are coupled to the rotor the total angular momentum will lie in the 2–3 plane. We call the solution planar, because $\boldsymbol{J}$ and the PA 2 and 3 lie in the same plane. At the band head, where $R = 0$, the angular momentum $\boldsymbol{J}$ is parallel to the 3-axis. With increasing spin it moves out into the 2–3 plane, as illustrated in the upper panel of Fig. 2. This type of solution has been found in Ref. [10]. If a high j proton particle and high j neutron hole (or vice versa) are coupled to the rotor, $\boldsymbol{J}$ will lie in the 1–3 plane at the band head and then gradually turn towards the 2-axis, as illustrated in the lower panel of Fig. 2. We call the solution aplanar, because $\boldsymbol{J}$ and any pair of PA do not lie in the same plane. Such type of solution has first been found in Ref. [8] on the basis of a microscopic TAC calculation, which assumes a fixed value of $\gamma = -30°$.

Fig. 3 shows the total Routhian $E'(\vartheta, \varphi)$ (Eq. (12)) for three selected values of the frequency ω. The motion of the minimum along the path illustrated in the lower panel of Fig. 2 can be seen.

Fig. 2 also shows the energies obtained from a numerical diagonalization of the PRM Hamiltonian (6). Fig. 4 compares the functions $I(\omega)$ derived from the PRM calculations with the ones obtained by TAC. There is rather good agreement between the two models. The TAC energies, which are not shown in Fig. 2, reproduce the PRM values very well. As discussed below, the kink of the function $I(\omega)$ represents a reorientation of the core angular momentum from the 3-axis or from the 1–3 plane towards the 2-axis.

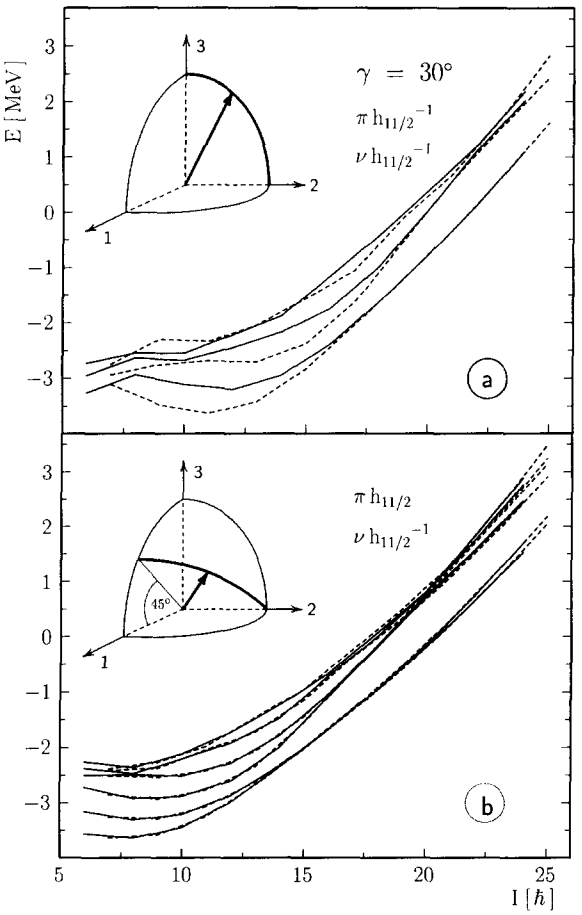

Fig. 2. Rotational levels of $h_{11/2}$ particles and holes coupled to a triaxial rotor with $\gamma = -30°$. The upper panel shows the case of a proton and a neutron hole and the lower panel the case of a proton particle and a neutron hole. Full lines correspond to even and dashed to odd spin.

3.1. Symmetries

The angles ϑ and φ, which specify the orientation of $\boldsymbol{J}$ in the intrinsic PA frame (cf. upper panel of Fig. 1), take only the discrete values satisfying the self-consistency condition $(\boldsymbol{J}|\boldsymbol{\omega})$. Due to the rotational symmetry of the two-body Hamiltonian H, there is a set of degenerate TAC solutions having the same values of the Euler angles ϑ and φ, but differing by the value of the angle ψ. The whole set of degenerate TAC solutions, $|\psi, \vartheta, \varphi\rangle$, is given by the different values the quadrupole moments Q_μ can take. The invariance of the intrinsic quadrupole moments Q'_0 and $(Q'_2 + Q'_{-2})/\sqrt{2}$ with respect to the rotations $\mathcal{R}_1(\pi)$, $\mathcal{R}_2(\pi)$ and $\mathcal{R}_3(\pi)$ (D_2 symmetry) restricts the Euler angles to $0 \leqslant \psi \leqslant 2\pi$, $0 \leqslant \vartheta \leqslant \pi/2$ and $0 \leqslant \varphi < \pi$. The other angles give values of Q_μ that are already included. One may see this also directly from Eq. (1) by using the symmetries of the D-functions and $Q'_2 = Q'_{-2}$. A superposition of TAC solutions $|\psi, \vartheta, \varphi\rangle$ with the

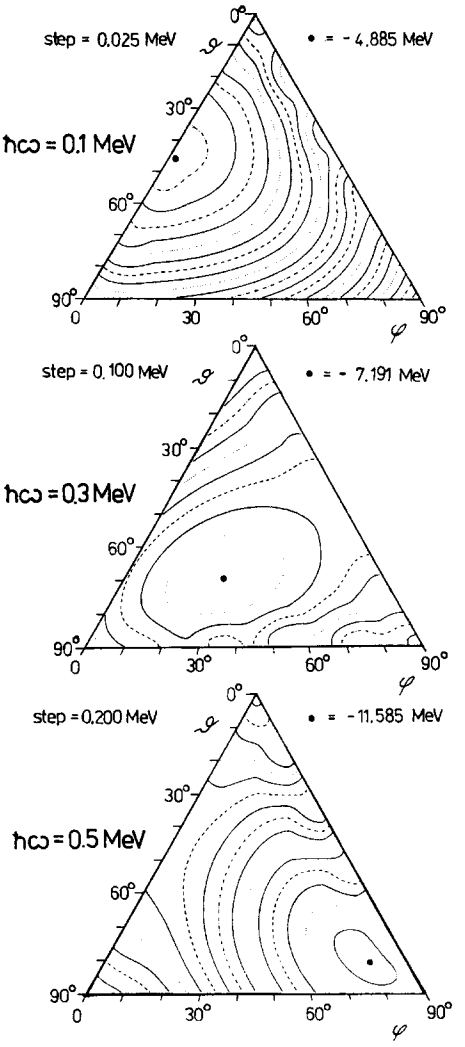

Fig. 3. Total Routhian (12) for a $h_{11/2}$ proton and a $h_{11/2}$ neutron hole coupled to a triaxial rotor with $\gamma = -30°$. The same coordinate system as in Ref. [8] is used: The coordinate lines $\vartheta = const$ are horizontal and the coordinate lines $\varphi = const$ connect the upper corner with the base line of the triangle. Wiggles of the contour lines are due to the numerical interpolation between the mesh points.

weight function $\exp(iI\psi)/\sqrt{2\pi}$ corresponds to a state of approximately good angular momentum $|I, M = I\rangle$ (approximate angular momentum projection).

One must distinguish between three cases:

(1) *PAC solution*

$$\vartheta = 0,\ \pi/2 \qquad \varphi = 0,\ \pi/2.$$

Then

$$|\psi + \pi, 0, 0\rangle = \mathcal{R}_3(\pi)|\psi, 0, 0\rangle = \mathrm{e}^{-i\alpha\pi}|\psi, 0, 0\rangle, \tag{13}$$

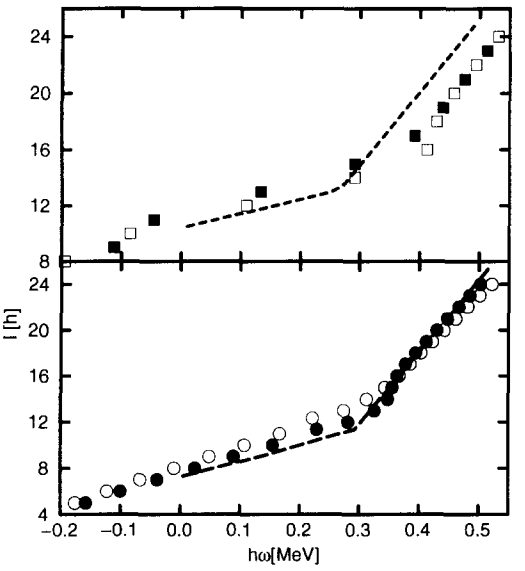

Fig. 4. The functions $I(\omega)$ for $h_{11/2}$ particles and holes coupled to a triaxial rotor with $\gamma = -30°$. The upper panel shows the case of a proton and a neutron hole and the lower panel the case of a proton particle and a neutron hole. The frequency is calculated by means of $\omega(I) = (E(I+1) - E(I-1))/2$ from the PRM energies in Fig. 2. In the upper panel the full squares are obtained from the odd spin yrast levels and the open squares from the even spin yrast levels. In the lower panel the open circles are obtained from the yrast band (both signatures) and the full circles from the yrare band (both signatures). Dashed lines correspond to the TAC calculations, where $I = J - 1/2$ is shown. For a discussion of the quantal correction 1/2, cf. Ref. [9].

$$|\psi + \pi, \pi/2, 0\rangle = \mathcal{R}_1(\pi)|\psi, \pi/2, 0\rangle = \mathrm{e}^{-i\alpha\pi}|\psi, \pi/2, 0\rangle, \tag{14}$$

$$|\psi + \pi, \pi/2, \pi/2\rangle = \mathcal{R}_2(\pi)|\psi, \pi/2, \pi/2\rangle = \mathrm{e}^{-i\alpha\pi}|\psi, \pi/2, \pi/2\rangle. \tag{15}$$

The signature α is a good quantum number and the values the total spin can take are restricted to $I = \alpha + 2n$.[3] The PAC solution represents one $\Delta I = 2$ band.

(2) *Planar TAC solution*

$$\vartheta \neq 0,\ \pi/2 \qquad \varphi = 0,\ \pi/2$$

or

$$\vartheta = \pi/2 \qquad \varphi \neq 0,\ \pi/2.$$

The signature symmetry is lost and all spins are possible. The planar TAC solution represents one $\Delta I = 1$ band.

(3) *Aplanar TAC solution*

$$\vartheta \neq 0,\ \pi/2 \qquad \varphi \neq 0,\ \pi/2.$$

The signature symmetry is lost and all spins are possible. There are *two* degenerate solutions $|\psi, \vartheta, \varphi\rangle$ and $|\psi, \vartheta, \pi/2 - \varphi\rangle$. The aplanar TAC solution represents two degenerate $\Delta I = 1$ bands.

[3] The selection rule follows from $\mathrm{e}^{iI\psi}|\psi, \vartheta, \varphi\rangle + \mathrm{e}^{iI(\psi+\pi)}|\psi + \pi, \vartheta, \varphi\rangle = (1 + \mathrm{e}^{i(I-\alpha)\pi})|\psi, \vartheta, \varphi\rangle$.

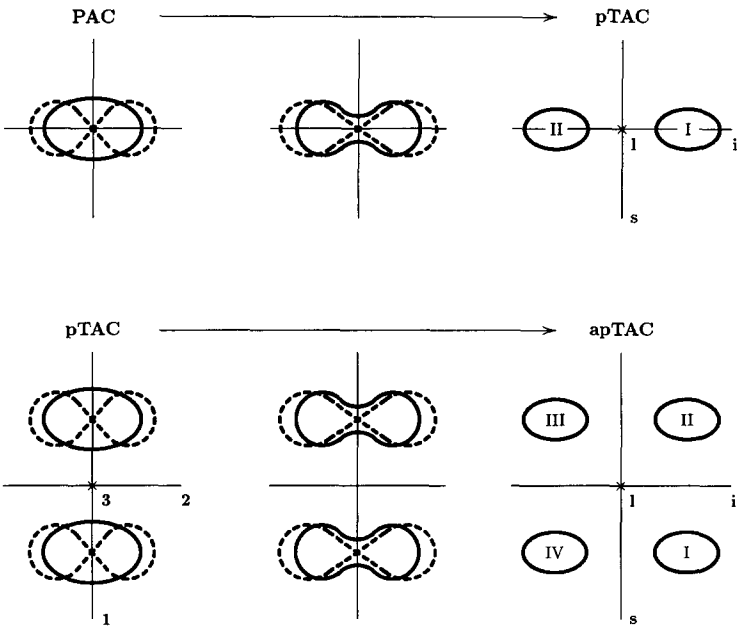

Fig. 5. Localization of the wave functions for PAC, planar TAC (pTAC) and aplanar TAC (apTAC) solutions. The full drawn ellipses symbolize the lowest solution at each position, which is symmetric. The dashed curves symbolize the first excited solution, which is odd.

Further insight into the nature of the symmetry breaking is gained by considering the orientation of $\boldsymbol{J}$ in the intrinsic frame. As discussed above, due to the D_2 symmetry it is sufficient to restrict $\boldsymbol{J}$ to the upper half space $\vartheta \geqslant \pi/2$. The topology of the solutions is illustrated in Fig. 5.

(1) *PAC solution*

$\boldsymbol{J}$ has the direction of the PA 3. The wave function is an eigenfunction of the rotation $\mathcal{R}_3(\pi)$ defining the signature of the corresponding $\Delta I = 2$ band.

(2) *Planar TAC solution*

$\boldsymbol{J}$ lies in one of the PP. There exists another degenerate solution constructed by the rotation $\mathcal{R}_3(\pi)$. The two solutions may be combined into two degenerate states of opposite signature that form one $\Delta I = 1$ band.

(3) *Aplanar TAC solution*

$\boldsymbol{J}$ does not lie in one of the PP. There are four degenerate solutions constructed by reflecting $\boldsymbol{J}$ on the 1–3 and 1–2 planes. They form a rectangle with the PA 3 in the center. The two solutions on each diagonal transform into each other by the rotation $\mathcal{R}_3(\pi)$. Each such pair can be combined into two degenerate states of opposite signature that form a $\Delta I = 1$ band. The two pairs correspond to two $\Delta I = 1$ bands.

The two bands representing an aplanar solution have an opposite intrinsic *chirality*. As seen in the lower panel of Fig. 6, the system formed by the short (s), intermediate (i) and long (l) semi-axes of the density distribution possess a chirality, when looking

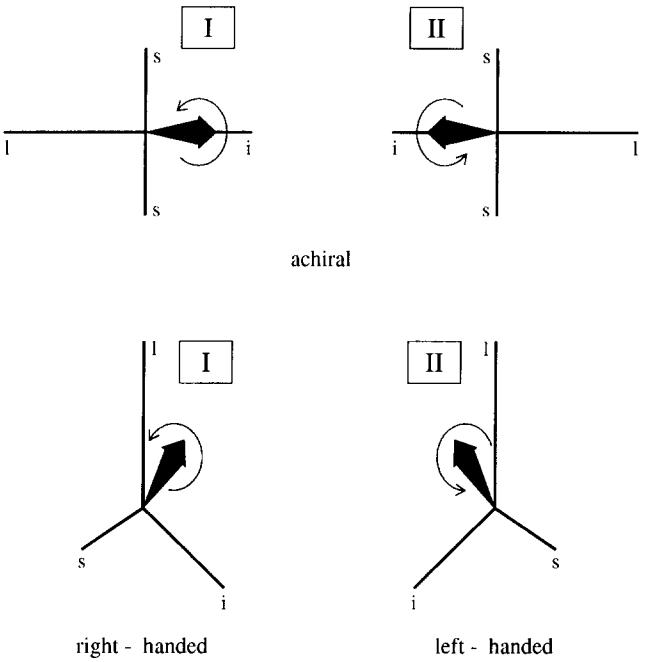

Fig. 6. Appearance of chirality for aplanar TAC solutions. The fat arrow represents the angular momentum $\boldsymbol{J}$. The solutions are labeled by the same Roman numerals as in Fig. 5.

from the tip of the angular momentum vector $\boldsymbol{J}$. If we agree to count in the order s, i, l, the solution I (first octant) is *right-handed*, i.e. the semi-axes s, i, l form a right-handed system. The solution II (second octant) is *left-handed*.

As seen in the upper panel of Fig. 6, there is no chirality defined if $\boldsymbol{J}$ lies in one of the PP (i–l in Fig. 6). Due to the D_{2h} symmetry the PA (s in Fig. 6) perpendicular to the PP is left–right symmetric. As a consequence, the solutions I and II are related to each other by a rotation by π about the $\boldsymbol{J}$ axis. In contrast, the solutions I and II in the lower panel of Fig. 6 cannot be transformed into each other by a rotation, because they have opposite chirality. Thus, aplanar TAC solutions are *chiral* and planar TAC solutions *achiral*. In the following we will prefer the terms "planar" and "chiral" to distinguish between the two types of solutions.

The name chirality is used following the terminology of chemistry (cf. e.g. Ref. [12]). Optical active molecules, which turn the polarization plane of light, have two stereo isomers, which are related to each other by reflection on a plane. These so-called enantiomers have opposite chirality. The example, most important to us, is the DNS helix, which forms a left-handed screw. The so-called "asymmetric C atom", to which four different substituents are bound, is an example for molecular chirality that comes closest to our case. Taking the bond to one substituent (e.g. the biggest one, the " rest of the molecule") as an axis (like the angular momentum in our case) the other three bonds form either a left-handed or a right-handed system (like the three semi-axes in our case).

It should be pointed out, though, that the chirality of molecules is of static nature. In the case of rotation the chirality is of dynamical origin, since it is only the angular momentum vector that defines a direction with respect to which the semi-axes s, i, l form a left- or right-handed system. The non-rotating nucleus has the D_{2h} symmetry of the triaxial density distribution, which is achiral.

One can express the symmetry also by saying that the sense of the physical rotation is the same as or opposite to the rotation an observer on $\boldsymbol{J}$ carries out, who first turns from the s - to the i-axis and then from the i - to the l-axis.

We have encountered a new kind of intrinsic symmetry breaking, which is not found among the symmetry types discussed by Bohr and Mottelson in Ref. [11], p. 19. Neither also it correspond to the case without any symmetry, since parity is still a good quantum number. We suggest the name "chiral doubling" for the appearance of the two identical bands in analogy to the "parity doubling" in the case of reflection asymmetric shapes [11]. In the latter case the two bands have opposite parity, though.

As examples for these general rules, let us discuss the triaxial TAC solutions of our model system. The planar case is illustrated in the upper panels of Figs. 2–6. Both the proton hole and the neutron hole tend to align with the 3-axis. First the core angular momentum $\boldsymbol{R}$ and, as a consequence, also $\boldsymbol{J}$ align with the 3-axis, because this orientation is favored by the Coriolis interaction. The solution is of PAC type. The bands of different signature, defined by the rotation $\mathcal{R}_3(\pi)$, are separated. They correspond to the different intrinsic states displayed by full and dashed lines in the upper panel of Fig. 5. For higher spin it is more efficient to increase the 2-component of $\boldsymbol{R}$, and $\boldsymbol{J}$ moves into the 2–3 plane. The two PAC solutions fission and develop into the two degenerate TAC solutions located symmetric to the 3-axis, which can be combined into two degenerate states of opposite signature. Accordingly, in the PRM calculation pairs of $\Delta I = 2$ sequences merge into $\Delta I = 1$ bands.

The kink of the function $I(\omega)$ seen in Fig. 4 is caused by the reorientation of $\boldsymbol{R}$ from the 3- towards the 2-axis. The larger core moment of inertia along the 2-axis leads to the increase of $\mathcal{J}^{(2)} = dI(\omega)/d\omega$, which is the slope of the curve $I(\omega)$. It is interesting to note that the reorientation of $\boldsymbol{R}$ is not a gradual process. It first remains parallel to the 3-axis before it reorients towards the 2-axis at the kink.

The chiral solution is shown in the lower panels of Figs. 2–6. The combination of the proton particle with the neutron hole favors the 1–3 plane. At low spin, $\boldsymbol{R}$ and $\boldsymbol{J}$ lie in the 1–3 plane, because this orientation minimizes the Coriolis interaction. There are two degenerate TAC solutions obtained by reflection on the 3-axis that can be combined into two degenerate states of opposite signature. Correspondingly, the low-spin PRM spectrum consists of $\Delta I = 1$ bands, which differ by the intrinsic wave functions of the proton and the neutron hole (full and dashed lines in the lower panel of Fig. 5). For higher spin it is again more efficient to increase the 2-component of $\boldsymbol{R}$, and $\boldsymbol{J}$ moves out of the 1–3 plane. The two planar TAC solutions fission into four aplanar ones. When they are sufficiently separated (tunneling is small), one can combine the four degenerate TAC solutions into two degenerate states of each signature. Accordingly, in Fig. 2 pairs of $\Delta I = 1$ bands merge into chiral doublets. The change of $\mathcal{J}^{(2)}$ in Fig. 4 again reflects

the reorientation of $\boldsymbol{R}$. The PRM states with the same value of I are somewhat split, indicating the presence of some tunneling between the left-handed and right-handed states.

3.2. Transition probabilities

The transition probabilities are calculated by means of the standard PRM expression, as given e.g. in Ref. [11] (cf. also Ref. [9]). For the M1 operator $g - g_R$ is set equal to 1 and -1 for the proton and the neutron hole, respectively. Only the rotor part of the E2 operator is taken and the intrinsic quadrupole moments are chosen as $Q_0' = \cos\gamma$ and $Q_2' = -\sin\gamma/\sqrt{2}$.

The TAC expressions for the reduced transition probabilities are the straightforward generalization of the ones for planar solutions (cf. e.g. Ref. [9]). For stretched M1 transitions one has

$$B(\mathrm{M1}) = \frac{3}{8\pi}\{[-\mu_3 \sin\vartheta + \cos\vartheta(\mu_1\cos\varphi + \mu_2 \sin\varphi)]^2 + [\mu_2\cos\varphi - \mu_1 \sin\varphi]^2\}, \tag{16}$$

where μ_ν are the intrinsic components of the expectation value of the operator of the magnetic moment,

$$\mu_\nu = \langle\hat{\mu}_\nu\rangle. \tag{17}$$

For stretched E2 transitions one has

$$B(\mathrm{E2}) = \frac{15}{128\pi}\left\{\left[Q_0'(\sin\vartheta)^2 + \sqrt{\frac{2}{3}}Q_2'(1 + (\cos\vartheta)^2)\cos 2\varphi\right]^2 + \frac{8}{3}\left[Q_2'\cos\vartheta \sin 2\varphi\right]^2\right\}. \tag{18}$$

In our model case, we use the same intrinsic quadrupole moments Q_0' and Q_2' as for the PRM and the magnetic moments are

$$\mu_\nu = \pm\langle j_\nu\rangle, \tag{19}$$

where the upper and lower signs hold for the proton and the neutron hole, respectively.

Fig. 7 shows the calculated reduced transition probabilities for the combination of a proton with a neutron hole. The inter band transition probabilities reflect the change from the planar to the aplanar rotation, which is illustrated in Fig. 5. At low spin there are transitions between the lowest and first excited states in the minimum in the 1–3 plane (full and dashed lines in Fig. 5). The distributions of the angular momenta are similar and can be connected by the E2 and M1 operators. The transitions from the excited to lowest band are stronger than the ones in the opposite direction. A similar phenomenon appears in PAC bands with a substantial signature splitting, where the M1 transitions

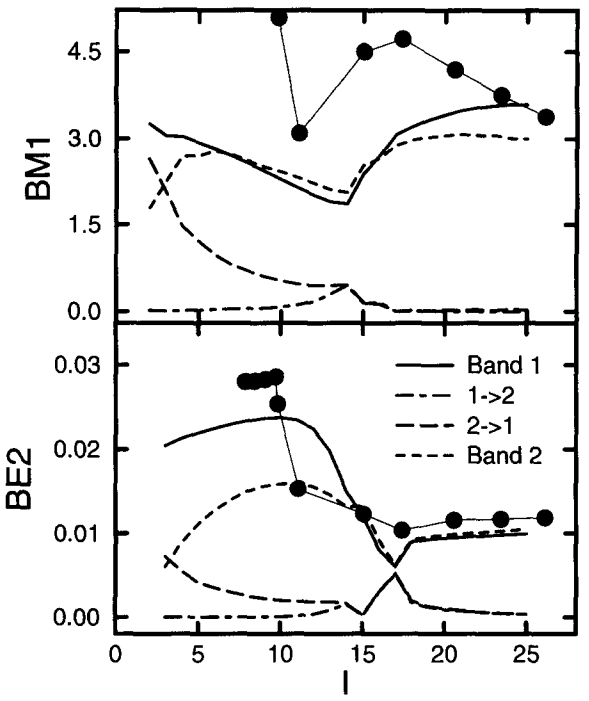

Fig. 7. $B(M1)$ and $B(E2)$ values from the particle rotor calculation for the case of a proton and a neutron hole coupled to the triaxial rotor.

are weak or strong, depending on whether the core angular momentum changes or not [13]. The inter band transitions disappear after the transition to the aplanar geometry near $I = 15$. The two degenerate solutions correspond to very different orientations of the angular momentum relative to the intrinsic frame, which cannot be connected by operators of low multipolarity, as M1 or E2. The origin of the K forbiddeness in axial nuclei may be viewed in the same way. Near $I = 15$, where the two bands in the PRM come very close, there is a mixing of the two intrinsic structures, which locally generates a maximum of the inter band and a minimum of the inter band transitions.

The TAC solutions reproduce the intra band transition probabilities between the yrast levels of the PRM calculation in a qualitative way. The deviation of TAC from PRM is stronger than in the axial case studied in Ref. [9]. The reason is probably that $\boldsymbol{R}$ may oscillate against $\boldsymbol{J}$, which is not possible for the axial rotor. The calculation of inter band transition probabilities is outside the realm of the TAC approach.

3.3. *Possible experimental evidence*

The case $\gamma = -30°$ is the most favorite one for the appearance of the chiral doublets. Fig. 8 shows the bands for a particle and a hole coupled to the triaxial rotor for different values of γ. The chiral doublets appear in the interval $25° < -\gamma < 40°$. Thus there is a certain margin of triaxiality, where the phenomenon can be expected. The two lowest

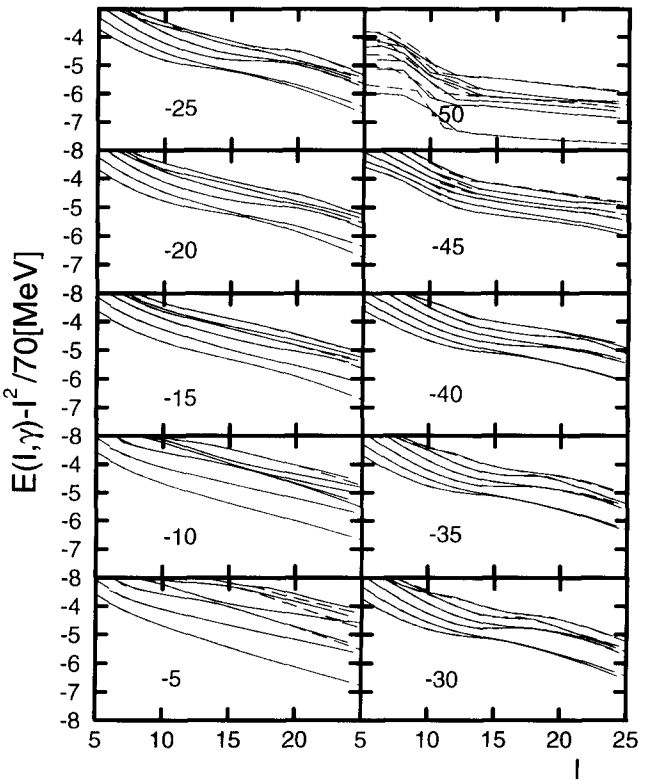

Fig. 8. Rotational levels of a $h_{11/2}$ proton and a $h_{11/2}$ neutron hole coupled to a triaxial rotor with different values of γ, which are indicated by the numbers in the panels. Full lines correspond to even and dashed to odd spin.

positive parity bands of ^{134}Pr, recently measured [15], are shown in Fig. 9. The assigned configuration for band 1 is a $h_{11/2}$ quasi proton combined with a $h_{11/2}$ quasi neutron, where the former has particle and the latter hole character. The spectrum is similar to our calculation for $\gamma = -20°$, showing a band crossing with the two bands staying close to each other later on. The transitions probabilities are qualitatively consistent with our calculation shown in Fig. 7: There are strong M1 and E2 crossover intra band transitions below the band crossing. The transitions from the excited (band 2) to the lowest band (band 1) are seen, where the ones in the opposite direction are missing (planar solution). Near the crossing transitions in both directions are seen (band mixing). Above the crossing no inter band transitions are observed. However, the population is too weak there to permit conclusions about the attenuation of the inter band transitions that is expected when approaching the chiral solution. In fact, the energy splitting of the two bands after the crossing suggests that there must be still substantial tunneling between the two chiralities. Thus, bands 1 and 2 in ^{134}Pr might correspond to a case close to the onset of the chirality. The situation reminds of the breaking of the reflection symmetry of the density distribution. In this case a number of bands with opposite parity have been found, which come close and cross, but do not merge into real parity doublets [16].

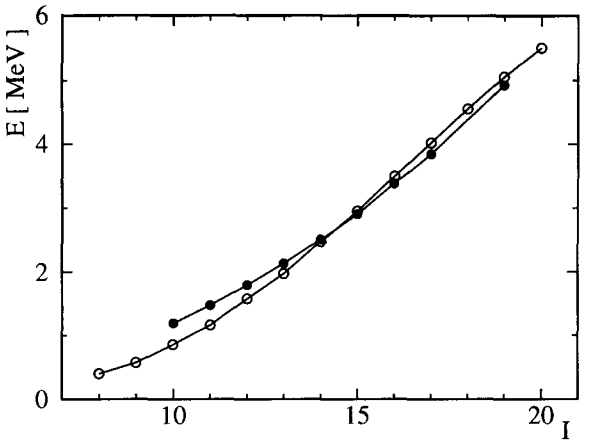

Fig. 9. Energy of the two lowest bands of positive parity in ^{134}Pm. The data is from Ref. [15], where band 1 (full dots) is assigned to the configuration of a $h_{11/2}$ quasi proton combined with a $h_{11/2}$ quasi neutron.

It is an open question whether sufficiently strong triaxiality occurs for the appropriate high j quasiparticle configurations, such that the genuine chiral doublets appear. The experimental evidence for triaxiality at low and medium spin can be understood assuming that nuclei in certain regions (e.g. mass 130 and 190) are soft with respect to triaxial deformations [14,17–19]. Thus, there is the question whether the assumed triaxiality of the aplanar TAC solution is really stable, as already pointed out in Ref. [8]. For a definite answer one has to carry out microscopic TAC calculations, based e.g. on the QQ-Hamiltonian (cf. Ref. [1] for the axial case), demanding also self-consistency with respect to the intrinsic quadrupole moments Q_0' and Q_2'. It is possible that due to the underlying microscopic structure the rotational energy of the core may depend in a more complex way on γ than in our model. For example, it has been demonstrated in Ref. [17] that quasiparticles from a half filled j prefer $\gamma = -30°$ and align with the 2-axis. The contribution of such quasiparticles to the core angular momentum could stabilize the chiral tilted rotation. It is also possible that at very high spin triaxial shapes are more stable, because they are favored by the liquid drop part of the energy (Jacobi instability). The appearance of chiral doublets would be a very clear signal for triaxial shapes. In order to answer these questions microscopic TAC calculations are necessary that are beyond the scope of the present paper and will be addressed in a forthcoming study.

4. Conclusions

Studying the model system of two particles coupled to a triaxial rotor, general features of tilted rotation in triaxial nuclei have been found that are distinctly different from the case of axial nuclei.

If high j holes are combined with a triaxial core the angular momentum will lie in the principal plane formed by the long and intermediate axes. For high j particles it

will lie in the principal plane formed by the short and intermediate axes. Such a planar TAC solutions correspond to a signature pair $\Delta I = 2$ bands that merges into a $\Delta I = 1$ band with increasing spin. This is different from typical axial nuclei where bands start as $\Delta I = 1$ sequences and develop a signature splitting with increasing spin.

If high j particles are combined with high j holes and with a triaxial core, the angular momentum will first lie in the principal plane defined by the short and long axis and with increasing spin be tilted towards the intermediate axis. The occurrence of such an aplanar solution corresponds to a pair of $\Delta I = 1$ bands that merges into a doublet $\Delta I = 1$ bands. The two degenerate $\Delta I = 1$ bands with the same parity correspond to opposite chirality of the end points of the three semi-axes of the triaxial density distribution relative to the angular momentum vector. This is a new type of symmetry breaking that is only possible in triaxial nuclei at high spin. The chiral doublets correspond to regular $\Delta I = 1$ bands with strong M1 and E2 intra band transition but no connecting inter band transitions.

Nuclei with mass around 190 and 130, which are known to be soft with respect to triaxial deformation, seem to be the most promising candidates to observe the chiral doublets. At present it is not clear whether the combination of high j intruder particles with high j intruder holes will permit a sufficiently stable triaxial deformation. The case studied in this paper, where the angular momentum components along the three axes arise from the high j intruder particles, collective core rotation and the high j intruder holes, is just one possibility for chiral TAC solutions. The angular momentum components along the three principal axes may also be generated by particle orbits with different geometry. An example could be a combination of high j intruder particles with mid shell high j intruder quasiparticles and normal parity high j holes.

Microscopic TAC calculations are necessary to decide whether the aplanar tilted rotation is stable and the chiral doublets exist. Independently, is seems interesting to look for chiral doublets in experiment. Bands 1 and 2 in ^{134}Pr reported in Ref. [15] might represent experimental evidence for an incipient chirality of the rotation.

Acknowledgements

Discussions with F. Dönau, B. Mottelson and P. Ring during the course of the work are gratefully acknowledged.

References

[1] S. Frauendorf, Nucl. Phys. A 557 (1993) 259c.
[2] S. Frauendorf and T. Bengtsson, AIP Conference Proceedings 259 (1992) 223.
[3] A. Brokstedt et al., Nucl. Phys. A 571 (1994) 337.
[4] J. B. Oliviera et al., Phys. Rev. C 50 (1994) 1360.
[5] F. Dönau et al., Nucl. Phys. A 548 (1994) 241.
[6] G. Baldsiefen et al., Nucl. Phys. A 574 (1994) 521.
[7] S. Frauendorf, Proc. Int. Conf. on Nucl. Structure at the Turn of the Century, Crete, July 1996, Z. Phys. A, in print.

[8] H. Frisk and R. Bengtsson, Phys. Lett. B 196 (1987) 14.
[9] S. Frauendorf and J. Meng, Z. Phys. A, in print.
[10] F.A. Dodaro and A.L. Goodman, Phys. Rev. C 49 (1994) 1482.
[11] A. Bohr and B. Mottelson, Nuclear Structure II (Benjamin, New York, 1975) p. 1.
[12] A. Streitwieser et al., Introduction to Organic Chemistry, third edition (Macmillan, New York, 1985) p. 113;
J. March, Advanced Organic Chemistry (Wiley, New York, 1992) p. 94.
[13] I. Hamamoto, Phys. Lett. B 102 (1981) 225.
[14] S. Frauendorf and F.R. May, Phys. Lett. B 125 (1983) 245.
[15] C.M. Petrache et al., Nucl. Phys. A 597 (1996) 106; private communication.
[16] I. Ahmad and P. Butler, Annu. Rev. Nucl. Part. Sci. 43 (1993) 71.
[17] Y.S. Chen et al., Phys. Rev. C 28 (1983) 2437.
[18] R. Wyss et al., Nucl. Phys. A 505 (1989) 337.
[19] P. v. Brentano et al., Proc. of Predeal Int. Summer School Collective Motion and Nuclear Dynamics, ed. A.A. Raduta et al., Romania 1995, and earlier work quoted therein.